Information Systems and Economics (2026)
Clausius Scientific Press, Canada
DOI: 10.23977/infse.2026.070115
ISSN 2523-6407 Vol. 7 Num. 1

Economic Dispatch of a Microgrid under Wind and Photovoltaic Uncertainty Based on Conditional Value-at-Risk and Multi-Strategy Adaptive Differential Evolution

Yanshuo Li

School of Economics, Nanjing University of Finance and Economics, Nanjing, China
18705183515@163.com

Keywords: Microgrids; Economic dispatch; Wind and solar uncertainties; Energy storage systems

Abstract: To address the issue of microgrid dispatch being susceptible to prediction bias under conditions of high wind and solar power integration, a risk-economic dispatch method based on Conditional Value-at-Risk (CVaR) and Multi-Strategy Adaptive Differential Evolution (MSDE) is proposed. First, a first-order autoregressive error model is used to describe the temporal correlation of wind and solar power prediction errors, generating multiple renewable energy output scenarios. Second, with energy storage charging and discharging power as the core decision variable, a risk adjustment objective function composed of expected operating cost and conditional value-at-risk is constructed, comprehensively considering grid interaction cost, micro gas turbine operating cost, diesel generator operating cost, carbon emission cost, energy storage degradation cost, and load shedding penalty. Finally, elite-guided mutation, adaptive parameter adjustment, local Gaussian search, and oppositional learning strategies are employed to improve the search efficiency of the differential evolution algorithm in multi-scenario dispatch. The 24-hour simulation results show that the proposed method achieves a risk adjustment target value of 3403.96 yuan, which is lower than that of the standard difference evolutionary algorithm and the particle swarm optimization (PSO) algorithm, while maintaining the energy storage state of charge (SOC) within the allowable range. Sensitivity analysis further shows that as the wind and solar forecast errors increase, the conditional risk value and cost fluctuations rise significantly, indicating that the proposed method can effectively balance the economic efficiency and uncertainty risks of microgrid operation.

1. Introduction

As the integration ratio of wind and solar power into microgrids continues to increase, microgrids are playing an increasingly important role in promoting renewable energy consumption [1-2], coordinating distributed power generation operations, and reducing system operating costs. However, wind speed, solar irradiance, and meteorological conditions exhibit significant randomness and volatility, making accurate prediction of wind and solar power output difficult [3-4]. When discrepancies exist between predicted and actual output, microgrids may experience power deficits, renewable energy surpluses, fluctuations in the state of charge (SOC) of energy storage, and increased power purchases from the main grid, thereby affecting the economic efficiency and stability of system operation. Therefore, when formulating microgrid dispatch plans, relying solely on deterministic wind and solar power forecasts is insufficient to meet the operational demands under conditions of high renewable energy integration; it is necessary to incorporate the uncertainties of wind and solar power output into the economic dispatch model.

To address the uncertainty of wind and solar power output, existing research typically describes the prediction error by constructing multiple possible renewable energy output scenarios and evaluates the operational effectiveness of dispatch schemes under different scenarios. These methods can intuitively reflect the impact of wind and solar power output changes on microgrid power balance and operating costs. However, if only the average operating cost under each scenario is used as the optimization objective, it may overlook unfavorable operating conditions with low probability of occurrence but significant economic losses. Conditional Value-at-Risk (CVaR) can reflect the average loss of high-cost scenarios at a certain confidence level. Introducing it into microgrid economic dispatch can improve the adaptability of dispatch schemes to large wind and solar forecast deviations while taking into account the economics of normal scenarios. Therefore, combining scenario analysis with Conditional Value-at-Risk is an effective way to handle wind and solar uncertainties and control operational risks.

Microgrid economic dispatch typically involves multiple decision variables such as energy storage charging and discharging power, controllable unit output, and main grid interaction power. It is also constrained by power balance, equipment capacity, unit ramping, and energy storage SOC, characterized by numerous variables, complex constraints, and a large search space. Intelligent optimization methods such as Particle Swarm Optimization (PSO) and Differential Evolution (DE) have been applied to microgrid scheduling problems because they do not rely on gradient information of the objective function. PSO has a simple structure, but it is prone to population diversity degradation and premature convergence in high-dimensional scheduling problems. Standard Differential Evolution has good global search capabilities, but its fixed differential weights and crossover probabilities make it difficult to simultaneously consider both early global exploration and later local optimization. When wind and solar uncertainties and risk objectives are simultaneously introduced, the computational complexity of the scheduling problem further increases, thus requiring improvements to the search strategy and parameter adjustment methods of Differential Evolution.

Based on the above analysis, this paper studies the economic scheduling problem of grid-connected microgrids considering the uncertainty of wind and solar power output, constructing a 24-hour scheduling model composed of wind power generation, solar power generation, micro gas turbines, diesel generators, energy storage systems, and the main grid. First, a time-dependent prediction error model is used to generate multiple wind and solar power output scenarios. The expected operating cost and conditional risk value of each scenario form the risk adjustment objective function, balancing average operating economics and the risks of high-cost scenarios. Second, a Multi-Strategy Adaptive Differential Evolution (MSDE) algorithm is proposed. Through elite-guided, adaptive parameter adjustment, local search, and population diversity preservation mechanisms, the algorithm's convergence speed and optimization accuracy are improved. Finally, a typical microgrid example is used to compare the proposed method with the Standard Differential Evolution algorithm and the Particle Swarm Optimization algorithm. The impact of different wind and solar prediction error levels on scheduling costs and operational risks is analyzed to verify the effectiveness of the established model and the proposed algorithm.

2. Microgrid Modeling and Problem Formulation

2.1. Microgrid Structure

The grid-connected microgrid considered in this study mainly consists of a wind generation unit, a photovoltaic generation unit, a microturbine, a diesel generator, a battery energy storage system, the utility grid, and an electrical load. Wind and photovoltaic generation are renewable energy sources and are preferentially utilized to supply the load under the premise of satisfying system operating constraints. The microturbine and diesel generator are controllable generation units that provide power compensation when renewable generation is insufficient. The battery energy storage system transfers energy among different time periods by charging during low-load or low-price periods and discharging during high-load or high-price periods. The utility grid further maintains the internal power balance of the microgrid through electricity purchasing and selling.

A two-stage scheduling framework is adopted to describe the coordinated operation of different devices. In the first stage, the 24-h battery charging and discharging schedule is determined and remains identical under all renewable generation scenarios. In the second stage, the outputs of the microturbine, diesel generator, and utility grid are adjusted according to the wind power, photovoltaic power, and net-load variations in each scenario. The scenario consistency constraint of the battery schedule is expressed as

$$P_{b,t}^{(1)} = P_{b,t}^{(2)} = \cdots = P_{b,t}^{(N_s)} = P_{b,t}, \quad \forall t \tag{1}$$

where $P_{b,t}$ denotes the battery power at time period t. A positive value represents discharging, whereas a negative value represents charging. This modeling approach ensures that the day-ahead battery schedule is determined before actual operation, while controllable generators and the utility grid are allowed to compensate for renewable generation deviations under different scenarios.

After defining the microgrid configuration and the coordination relationship among its components, the uncertainty of wind and photovoltaic generation should first be modeled to provide uncertain inputs for the subsequent scenario-based dispatch process.

2.2. Wind and Photovoltaic Generation Uncertainty Model

Wind and photovoltaic generation are affected by wind speed, solar irradiance, and weather conditions, and their actual outputs generally deviate from day-ahead forecasts. The wind and photovoltaic outputs at time period t under scenario s are represented as the sum of the forecast value and the forecast error [5-6]:

$$P_{pv,t}^{(s)} = \hat{P}_{pv,t} + \varepsilon_{pv,t}^{(s)} \tag{2}$$

$$P_{w,t}^{(s)} = \hat{P}_{w,t} + \varepsilon_{w,t}^{(s)} \tag{3}$$

where $\hat{P}_{w,t}$ and $\hat{P}_{pv,t}$ denote the forecast wind and photovoltaic power at time period t, respectively. $P_{w,t}^{(s)}$ and $P_{pv,t}^{(s)}$ denote the wind and photovoltaic outputs under scenario s, while $\varepsilon_{w,t}^{(s)}$ and $\varepsilon_{pv,t}^{(s)}$ represent the corresponding forecast errors.

If mutually independent random errors are directly adopted, the renewable output may exhibit abrupt variations between adjacent time periods that are inconsistent with actual operating characteristics. To preserve the temporal continuity of forecast errors, a first-order autoregressive error model is used to generate wind and photovoltaic scenarios [7-8]:

$$\varepsilon_{r,t}^{(s)} = \rho_r \varepsilon_{r,t-1}^{(s)} + \sigma_{r,t} \sqrt{1-\rho_r^2}\, z_{r,t}^{(s)}, \quad r \in \{w, pv\} \tag{4}$$

where $r$represents wind or photovoltaic generation, $\rho_r$is the temporal correlation coefficient of the forecast error, $\sigma_{r,t}$denotes the error standard deviation at time period t, and $z_{r,t}^{(s)}$is a random variable following the standard normal distribution. A larger $\rho_r$indicates stronger temporal continuity between forecast errors in adjacent periods.

Considering that wind and photovoltaic outputs cannot be negative or exceed their installed capacities, the scenario output is constrained as

$$P_{r,t}^{(s)} = \min\left\{P_r^{\max}, \max\left[0, \hat{P}_{r,t} + \varepsilon_{r,t}^{(s)}\right]\right\}, \quad r \in \{w, pv\} \tag{5}$$

If all scenarios are assumed to have equal probabilities, the scenario probability is given by

$$\pi_s = \frac{1}{N_s}, \quad \sum_{s=1}^{N_s} \pi_s = 1 \tag{6}$$

Variations in wind and photovoltaic generation directly cause fluctuations in the microgrid net load. Therefore, controllable generation units are required to compensate for renewable power shortages. The operating models of the microturbine and diesel generator are established in the following subsections.

2.3. Microturbine Model

The microturbine has the advantages of rapid response, a wide regulation range, and stable operation. It can supply part of the load when renewable generation is insufficient or the electricity price is relatively high. The operating cost of the microturbine under scenario $s$consists of fuel and operation and maintenance costs:

$$C_{MT}^{(s)} = \sum_{t=1}^{T} \left(c_{MT}^{f} + c_{MT}^{om}\right) P_{MT,t}^{(s)} \Delta t \tag{7}$$

where $P_{MT,t}^{(s)}$is the microturbine output power at time period $t$under scenario s, c_{MT}^{f}denotes the unit fuel cost, c_{MT}^{om}denotes the unit operation and maintenance cost, and $\Delta t$is the scheduling interval.

The microturbine output is subject to the capacity constraint:

$$0 \le P_{MT,t}^{(s)} \le P_{MT}^{\max} \tag{8}$$

To prevent excessive power variations between adjacent periods, the ramping constraint is expressed as

$$-R_{MT} \le P_{MT,t}^{(s)} - P_{MT,t-1}^{(s)} \le R_{MT} \tag{9}$$

where $P_{MT}^{\max}$is the maximum output power of the microturbine and $R_{MT}$is the maximum allowable ramping power between adjacent periods.

2.4. Diesel Generator Model

The diesel generator is characterized by flexible start-up and reliable power supply. It mainly compensates for the remaining load when the available power from the microturbine, battery, and utility grid is insufficient. Because the diesel generator generally has relatively high fuel costs and pollutant emissions, its output should be reasonably limited while maintaining system reliability.

The operating cost of the diesel generator is expressed as

$$C_{DG}^{(s)} = \sum_{t=1}^{T} \left(c_{DG}^{f} + c_{DG}^{om}\right) P_{DG,t}^{(s)} \Delta t \tag{10}$$

where $P_{DG,t}^{(s)}$ is the diesel generator output power, while c_{DG}^{f} and c_{DG}^{om} denote the unit fuel cost and operation and maintenance cost, respectively.

The output constraint of the diesel generator is

$$0 \le P_{DG,t}^{(s)} \le P_{DG}^{\max} \tag{11}$$

The ramping constraint of the diesel generator is

$$-R_{DG} \le P_{DG,t}^{(s)} - P_{DG,t-1}^{(s)} \le R_{DG} \tag{12}$$

where $P_{DG}^{\max}$ is the maximum diesel generator output and R_{DG} is the maximum ramping power.

Although the microturbine and diesel generator can compensate for renewable generation shortages, excessive reliance on controllable generators increases fuel costs and carbon emissions. To improve renewable energy utilization and reduce load fluctuations, the battery energy storage model is further introduced.

2.5. Battery Energy Storage System Model

The battery energy storage system transfers energy among different time periods by changing its charging and discharging states. In this paper, a positive battery power $P_{b,t}$ represents discharging, while a negative value represents charging. For convenience, the positive-part function is defined as

$$[x]^{+} = \max(x, 0) \tag{13}$$

Considering charging and discharging efficiencies, the state-of-charge variation is expressed as

$$SOC_{t+1} = SOC_t + \frac{\eta_{ch}[-P_{b,t}]^{+}\Delta t}{E_b} - \frac{[P_{b,t}]^{+}\Delta t}{\eta_{dis}E_b} \tag{14}$$

where SOC_t denotes the beginning of time period t, E_b is the rated battery capacity, and η_{ch} and η_{dis} are the charging and discharging efficiencies, respectively.

The battery charging and discharging power is constrained by

$$-P_b^{\max} \le P_{b,t} \le P_b^{\max} \tag{15}$$

The battery SOC should remain within its allowable range:

$$SOC^{\min} \le SOC_t \le SOC^{\max} \tag{16}$$

To prevent excessive battery discharge at the end of the scheduling horizon and ensure energy continuity between adjacent scheduling cycles, the terminal state-of-charge constraint is given by

$$\left|SOC_T - SOC_0\right| \le \delta_{SOC} \tag{17}$$

where δ_{SOC} is the allowable deviation of the terminal SOC.

Frequent charging and discharging accelerate battery degradation. Therefore, a linear cost related to battery energy throughput is adopted to represent battery degradation:

$$C_b = c_b \sum_{t=1}^{T} \left|P_{b,t}\right| \Delta t \tag{18}$$

where c_b is the battery degradation cost coefficient per unit of charging or discharging energy.

2.6. Utility Grid Interaction and Power Balance Constraints

A positive utility grid power $P_{g,t}^{(s)}$ represents electricity purchased by the microgrid, while a negative value represents electricity sold to the utility grid. The grid interaction power is constrained by

$$-P_g^{sell,\max} \le P_{g,t}^{(s)} \le P_g^{buy,\max} \tag{19}$$

where $P_g^{buy,\max}$ and $P_g^{sell,\max}$ denote the maximum purchasing and selling powers, respectively.

The utility grid interaction cost consists of the electricity purchasing cost and selling revenue:

$$C_g^{(s)} = \sum_{t=1}^{T}\left[c_t^{buy}[P_{g,t}^{(s)}]^+ - c_t^{sell}[-P_{g,t}^{(s)}]^+\right]\Delta t \tag{20}$$

where c_t^{buy} and c_t^{sell} denote the electricity buying and selling prices at time period t, respectively.

The microgrid must satisfy the power balance constraint under every scenario and at each time period:

$$P_{w,t}^{(s)} + P_{pv,t}^{(s)} + P_{MT,t}^{(s)} + P_{DG,t}^{(s)} + P_{g,t}^{(s)} + P_{b,t} + P_{shed,t}^{(s)} = P_{L,t} + P_{curt,t}^{(s)} \tag{21}$$

where $P_{L,t}$ denotes the load demand at time period t, $P_{shed,t}^{(s)}$ denotes the load-shedding power, and $P_{curt,t}^{(s)}$ denotes the renewable curtailment power. Both variables satisfy the non-negativity constraints:

$$P_{shed,t}^{(s)} \ge 0, \qquad P_{curt,t}^{(s)} \ge 0 \tag{22}$$

By introducing load-shedding and renewable curtailment variables, the power balance equation remains feasible even under extreme renewable generation scenarios. Meanwhile, a sufficiently high load-shedding penalty is incorporated into the objective function so that load shedding occurs only when internal generation and utility grid regulation are both insufficient.

After establishing the component models and power balance constraints, the economic cost, environmental cost, and renewable curtailment cost of the microgrid are further formulated in a unified manner.

2.7. Scenario-Based Operating Cost Model

The carbon emissions under scenario s mainly arise from utility grid purchases, microturbine generation, and diesel generator operation. The total carbon emissions are expressed as

$$E^{(s)} = \sum_{t=1}^{T}\left[\mu_g[P_{g,t}^{(s)}]^+ + \mu_{MT}P_{MT,t}^{(s)} + \mu_{DG}P_{DG,t}^{(s)}\right]\Delta t \tag{23}$$

where μ_g, μ_{MT}, and μ_{DG} denote the carbon emission coefficients of utility grid purchases, microturbine generation, and diesel generation, respectively.

Accordingly, the total operating cost under scenario s is formulated as

$$alignedC^{(s)} = C_g^{(s)} + C_{MT}^{(s)} + C_{DG}^{(s)} + C_b + c_e E^{(s)} + c_{curt}\sum_{t=1}^{T}P_{curt,t}^{(s)}\Delta t + c_{shed}\sum_{t=1}^{T}P_{shed,t}^{(s)}\Delta t \tag{24}$$

where c_e denotes the unit carbon emission cost, c_{curt} denotes the renewable curtailment penalty coefficient, and c_{shed} denotes the load-shedding penalty coefficient.

This setting indicates that supply reliability has a higher priority than renewable energy utilization and prevents the optimization algorithm from reducing the total cost through intentional load shedding.

The expected operating cost over all scenarios is expressed as

$$\mathrm{E}[C]=\sum_{s=1}^{N_s}\pi_s C^{(s)} \tag{25}$$

The expected operating cost reflects the average economic performance of the dispatch solution over all scenarios. However, it may weaken the influence of a small number of high-cost scenarios. Therefore, conditional value-at-risk is further introduced to quantify the tail economic risk caused by wind and photovoltaic forecast errors.

2.8. CVaR-Based Objective Function

CVaR is used to quantify the average loss of high-cost scenarios beyond a specified confidence level [9-10]. Let αdenote the confidence level and ηdenote the Value-at-Risk of the cost distribution at confidence level α. The CVaR is expressed as

$$CVaR_\alpha(C)=\min_\eta\left[\eta+\frac{1}{1-\alpha}\sum_{s=1}^{N_s}\pi_s\left[C^{(s)}-\eta\right]^+\right] \tag{26}$$

where $\left[C^{(s)}-\eta\right]^+$denotes the cost exceeding the Value-at-Risk threshold under scenario s. A larger confidence level αplaces greater emphasis on extreme scenarios in the tail of the cost distribution.

To simultaneously account for average operating economy and high-cost scenario risk, the expected operating cost and CVaR are combined to formulate the following risk-adjusted objective function:

$$\min F=\mathrm{E}[C]+\lambda CVaR_\alpha(C) \tag{27}$$

where $\lambda$is the risk-weighting coefficient. When $\lambda=0$, the model only minimizes the average operating cost over all renewable generation scenarios. As λincreases, the dispatch strategy pays more attention to high-cost scenarios and tends to retain additional regulation capability from controllable generators and the battery energy storage system.

In summary, the proposed risk-aware microgrid economic dispatch model is formulated as

$$F=\sum_{s=1}^{N_s}\pi_s C^{(s)}+\lambda CVaR_\alpha(C) \tag{28}$$

3. Proposed Multi-Strategy Adaptive Differential Evolution Method

3.1. Decision Variable Encoding

The 24-h battery charging and discharging powers are selected as the main decision variables. Each individual represents a complete battery scheduling scheme and is encoded as

$$X_i=\left[P_{b,1}^i,P_{b,2}^i,\ldots,P_{b,T}^i\right] \tag{29}$$

where $X_i$denotes the i-th individual in the population, and $P_{b,t}^i$denotes the battery power at time period t. In this study, $T=24$, so each individual contains 24 decision variables. A positive value represents battery discharging, whereas a negative value represents battery charging. The battery power satisfies

$$-P_b^{\max}\le P_{b,t}^i\le P_b^{\max} \tag{30}$$

After a battery schedule is specified, the utility grid power, microturbine output, and diesel generator output are determined according to the scenario-based net load, marginal generation costs, device capacities, and ramping constraints. This encoding method reduces the number of directly optimized variables and therefore lowers the computational complexity of the multi-scenario dispatch problem.

3.2. Elite-Guided Mutation Strategy

The standard differential evolution algorithm usually selects individuals randomly for mutation. Although this mechanism helps maintain population diversity, it provides limited guidance toward promising regions. To improve the search direction, an elite-guided mutation strategy is adopted [11-12]:

$$V_i^g = X_i^g + F_i^g\left(X_{pbest}^g - X_i^g\right) + F_i^g\left(X_{r1}^g - X_{r2}^g\right) \tag{31}$$

where g is the current generation, V_i^g is the mutant vector generated for the i-th individual, X_{pbest}^g is randomly selected from the better-performing individuals in the current population, X_{r1}^g and X_{r2}^g are two distinct randomly selected individuals, and F_i^g is the differential weight.

A relatively large elite subset is used in the early search stage to preserve diversity. As the iteration proceeds, the elite range is gradually reduced so that the algorithm can focus more strongly on high-quality regions.

To avoid excessive dependence on elite individuals, the standard random mutation strategy is also employed with a certain probability:

$$V_i^g = X_{r1}^g + F_i^g\left(X_{r2}^g - X_{r3}^g\right) \tag{32}$$

The combined use of the two mutation strategies achieves a balance between elite guidance and population diversity.

3.3. Adaptive Control Parameters

The differential weight F and crossover probability CR have significant effects on the search performance of differential evolution. A larger differential weight is favorable for global exploration, whereas a smaller value is more suitable for fine local search [13-14]. Therefore, the differential weight is gradually reduced with the iteration process:

$$F_g = F_{\max} - \left(F_{\max} - F_{\min}\right)\frac{g}{G} \tag{33}$$

where G is the maximum number of generations, and $F_{\max}$ and $F_{\min}$ are the upper and lower bounds of the differential weight.

The crossover probability is gradually increased as

$$CR_g = CR_{\min} + \left(CR_{\max} - CR_{\min}\right)\frac{g}{G} \tag{34}$$

In the actual update process, random perturbations are introduced around F_g and CR_g, allowing different individuals to use different control parameters and improving the adaptability of the algorithm at different search stages.

After parameter updating, binomial crossover is applied to generate the trial vector:

$$U_{i,j}^{g} = \begin{cases} V_{i,j}^{g}, & rand_j \le CR_i^g \ \textbf{or} \ j = j_{rand} \\ X_{i,j}^{g}, & \textbf{otherwise} \end{cases} \tag{35}$$

where $U_{i,j}^{g}$ is the j-th component of the trial vector, and j_{rand} ensures that the trial vector contains at least one component from the mutant vector.

3.4. Local Gaussian Search

During the later iterations, the population may converge slowly around the current best solution. To improve local search accuracy, Gaussian perturbation is periodically applied to the current best individual [15]:

$$X_{new}^{g} = X_{best}^{g} + \mathrm{N}\left(0, \sigma_g^2\right) \tag{36}$$

where X_{best}^{g} denotes the best individual in generation g, and σ_g is the perturbation intensity. As the number of iterations increases, σ_g is gradually reduced, allowing the search to shift from relatively broad local exploration to fine exploitation.

If the newly generated individual has a better objective value than the current best individual, it replaces the original best solution. This strategy improves the accuracy of the obtained battery scheduling scheme.

3.5. Opposition-Based Learning Strategy

To prevent the population from becoming trapped in a local optimum, an opposition-based learning strategy is introduced. For the current best individual, its opposite solution is defined as

$$X_{opp}^{g} = X^{\min} + X^{\max} - X_{best}^{g} \tag{37}$$

where $X^{\min}$ and $X^{\max}$ denote the lower and upper bounds of the decision variables, respectively.

To make the opposite solution more consistent with battery scheduling characteristics, it is combined with a heuristic battery schedule derived from time-of-use electricity prices:

$$X_{opp}^{g} = \omega X_{opp}^{g} + (1-\omega) X_h \tag{38}$$

where X_h is the heuristic battery schedule and ω is the combination weight. If the generated opposite individual performs better than a poor individual in the current population, the latter is replaced. This mechanism expands the effective search range of the population.

3.6. Fitness Evaluation and Selection

For each trial individual, the battery state-of-charge trajectory is first calculated. The microturbine, diesel generator, and utility grid powers are then dispatched under all wind and photovoltaic scenarios. The fitness value is evaluated according to the expected operating cost and Conditional Value-at-Risk:

$$f(X_i) = \mathrm{E}\left[C(X_i)\right] + \lambda CVaR_{\alpha}\left[C(X_i)\right] + \Phi(X_i) \tag{39}$$

where $\Phi(X_i)$ denotes the constraint penalty term, mainly including penalties for state-of-charge violations and terminal state-of-charge deviations.

A greedy selection mechanism is adopted between the parent and trial individuals:

$$X_i^{g+1} = \begin{cases} U_i^g, & f(U_i^g) < f(X_i^g) \\ X_i^g, & \textbf{\textit{otherwise}} \end{cases} \tag{40}$$

By retaining the individual with the better fitness value, the best objective value of the population is prevented from deteriorating during the iterative process.

4. Case Analysis and Results

4.1. Case Parameter Settings

To verify the effectiveness of the established microgrid risk-economic dispatch model and multi-strategy adaptive differential evolution algorithm, this paper selects a grid-connected microgrid for a 24-hour day-ahead dispatch study, with a dispatch interval of 1 hour. The system consists of wind power generation units, photovoltaic power generation units, micro gas turbines, diesel generators, battery energy storage systems, a public grid, and electrical loads. The example data is constructed based on typical microgrid source-load variations and time-of-use pricing characteristics to analyze the power coordination relationships among various devices under different wind and solar power output scenarios.

The battery energy storage system has a rated capacity of 500 kWh, a maximum charge/discharge power of 120 kW, an initial SOC of 0.55, and an allowable range of 0.20–0.90. The maximum output power of the micro gas turbine and diesel generator are 240 kW and 180 kW, respectively. The maximum power purchased and sold between the microgrid and the main grid are 180 kW and 250 kW, respectively. The baseline error level for wind and solar power predictions is set at 10%, and 40 power output scenarios with the same probability of occurrence are generated. The confidence level for CVaR was set at 0.90, and the risk weighting coefficient was set at 0.20.

4.2. Source-Load Curves and Uncertainty Analysis of Wind and Solar Power

The day-ahead power curves for wind power, solar power, and load are shown in Figure 1. Load power is at a low level at night, gradually increasing thereafter, forming two relatively obvious load peaks around 11:00 and 17:00. The maximum daily load is 690 kW, and the minimum load is 270 kW. Solar power output is mainly concentrated between 7:00 and 19:00, peaking at 13:00; wind power output is present throughout the day, showing an overall trend of first decreasing and then increasing. The temporal complementarity of wind and solar power can reduce the net load of the microgrid to some extent, but it still cannot completely cover the power demand during the high-load periods in the morning and evening.

The time-of-use electricity purchase and sale prices are shown in Figure 2. The period from 1:00 to 7:00 is a low-price period, 11:00 to 12:00 and 18:00 to 21:00 are high-price periods, and the remaining time is a flat-price period. The retail electricity price changes synchronously with the purchase price, but is always lower than the purchase price. This pricing mechanism guides energy storage systems to absorb electricity during periods of low electricity prices and release it during periods of high electricity prices and high load, thereby reducing the main grid's electricity purchase cost for microgrids.

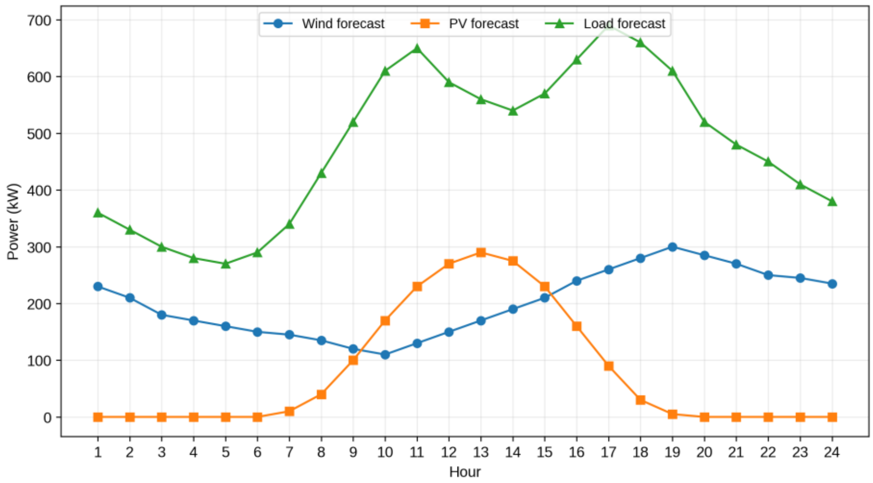

Figure 1: Day-ahead power curves of wind power, solar power and load.

Figure 2: Time-of-use electricity pricing.

Figure 3 shows the mean and 90% range for wind and solar power scenarios. Wind power scenarios exhibit some fluctuation throughout the day, while solar power uncertainty is mainly concentrated during daytime periods with sunlight. The range of variation in wind and solar power scenarios increases accordingly when the predicted power is higher. Because this paper uses a prediction error model with time correlation, the changes in renewable energy output between adjacent time periods have good continuity, avoiding unreasonable power spikes caused by independent random errors. The resulting scenarios can provide information on renewable energy output deviations of varying degrees for risk-based economic dispatch.

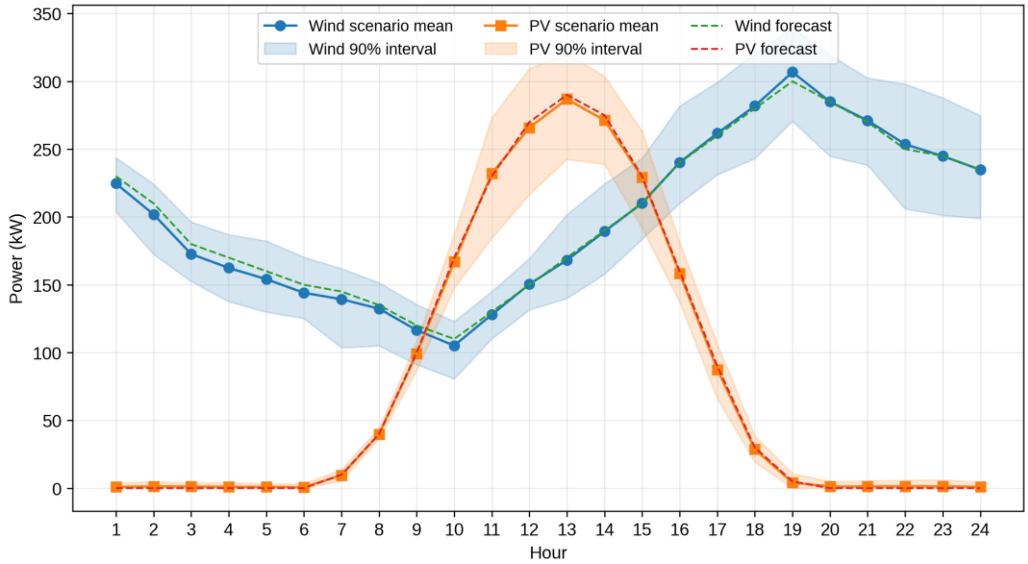

Figure 3: Uncertainty Analysis.

4.3. Microgrid Optimal Dispatch Results

The optimal power dispatch results of the microgrid, obtained using the proposed multi-strategy adaptive differential evolution algorithm, are shown in Figure 4. During each time period, wind and solar power are prioritized to meet load demand, with the remaining power deficit compensated by battery energy storage systems, micro gas turbines, diesel generators, and the public grid.

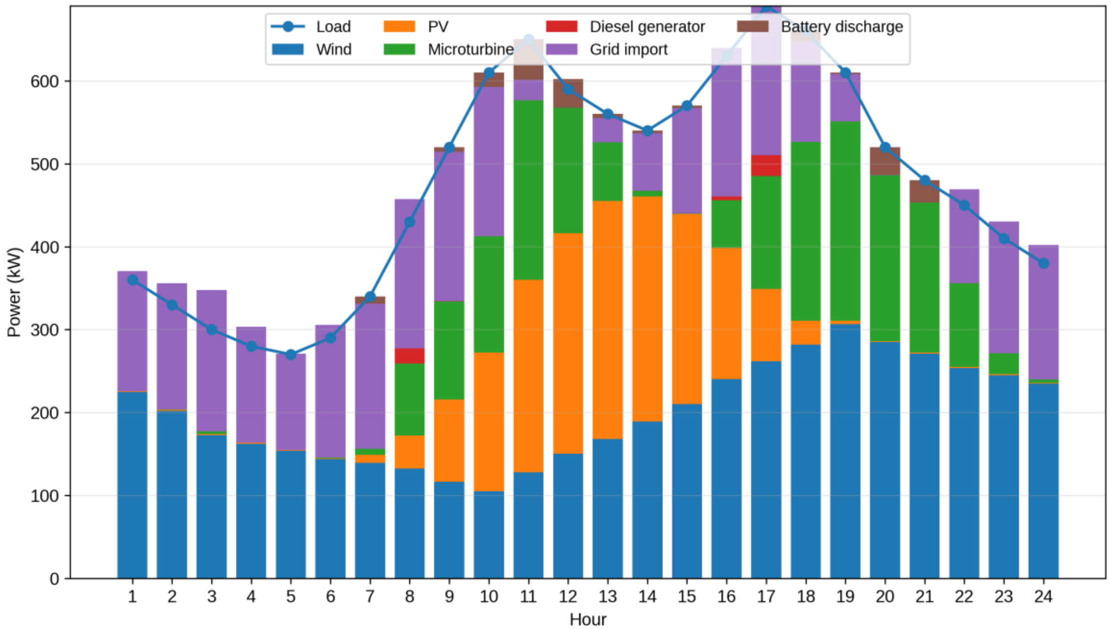

Figure 4: Typical daily attack rate dispatch results of microgrids.

From 1:00 to 6:00, both load and electricity purchase price are at low levels. The system mainly utilizes grid power to meet the remaining load and charge the energy storage system. From 8:00 to 10:00, the load increases rapidly, while solar power output has not yet reached a high level. Grid power purchase approaches the 180 kW upper limit, and micro gas turbines and a small number of diesel generators begin to contribute to power supply. From 11:00 to 12:00, solar power output increases significantly, and electricity prices enter peak periods. The energy storage system switches to discharging, and micro gas turbines assume the main controllable power output, thus reducing the need for high-priced grid power purchases.

From 13:00 to 15:00, the total output of wind and solar power is high, and the output power of micro gas turbines decreases significantly. At 12:00, some surplus power was sold to the main grid via the interconnection line. From 16:00 to 17:00, as photovoltaic output decreased and load increased again, the main grid purchased electricity, micro gas turbines, and diesel generators jointly compensated for the power shortage. From 18:00 to 21:00, during the high-price period in the evening, the energy storage system continuously discharged, and the output of the micro gas turbines increased, reaching a maximum power of 240 kW at 19:00, thereby reducing dependence on high-priced electricity purchases.

Under the baseline wind and solar power error level, the system's net purchased electricity was 2809.25 kWh, the micro gas turbine power generation was 1962.65 kWh, and the diesel generator power generation was only 48.68 kWh. The diesel generators only provided supplementary power during a few periods of power shortage, indicating that the optimization results can prioritize the use of the main grid and micro gas turbines with lower marginal costs. No wind or solar curtailment or load shedding occurred throughout the entire dispatch cycle, and all types of power sources were able to jointly meet the load demand, verifying the feasibility of the dispatch scheme.

4.4. Energy Storage System Operation Results

Figure 5 shows the changes in energy storage charging and discharging power and state of charge (SBC). A negative value indicates charging, and a positive value indicates discharging. The results show that the energy storage system mainly charges during the low-price period from 1:00 AM to 6:00 AM and discharges during the high-price periods from 11:00 AM to 12:00 PM and from 6:00 PM to 9:00 PM. The overall operating pattern is consistent with the time-of-use electricity price and net load changes.

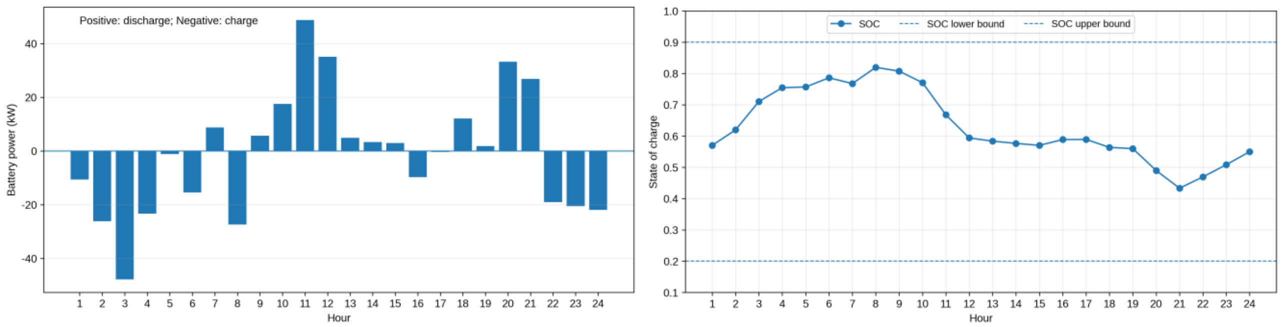

(a) Energy storage charging and discharging power (b) Changes in state of charge

Figure 5: Energy storage system operation performance.

The initial SBC of the energy storage was 0.55. After continuous charging in the early stages, it gradually increased, reaching a maximum of 0.820 at 8:00 AM. With the discharge during the high-load periods at noon and in the evening, the SBC gradually decreased, reaching a minimum of 0.433 at 9:00 PM. Subsequently, the energy storage recharged from 10:00 PM to midnight, eventually restoring the SBC to 0.550, essentially consistent with the initial state.

Throughout the entire dispatch cycle, the energy storage SBC remained within the allowable range of 0.20 to 0.90, without any exceeding of the limit. The state of charge at the end of the circuit is close to the initial value, indicating that the dispatch scheme did not gain a short-term cost advantage by excessively consuming energy storage capacity, and can reserve reasonable available capacity for the next dispatch cycle. At the same time, the energy storage degradation cost is 19.11 yuan, which is a low proportion of the total cost, indicating that the energy storage system did not engage in excessively frequent charging and discharging while participating in peak shaving and valley filling.

4.5. Comparison of Different Optimization Algorithms

The convergence process of different algorithms is shown in Figure 6, and the corresponding scheduling results are shown in Table 1 and Figure 7. The Standard Difference Evolution algorithm shows relatively small improvement under the current parameter settings, ultimately settling at a relatively high objective function value. The Particle Swarm Optimization algorithm gradually improves the quality of the solution in the middle of the iteration, but the rate of decrease slows down in the later stages. The proposed multi-strategy adaptive differential evolution algorithm maintains the population search range in the early stages and achieves a significant decrease in the objective function in the later stages through elite guidance, local Gaussian search, and adversarial learning, ultimately obtaining the best result among the three methods.

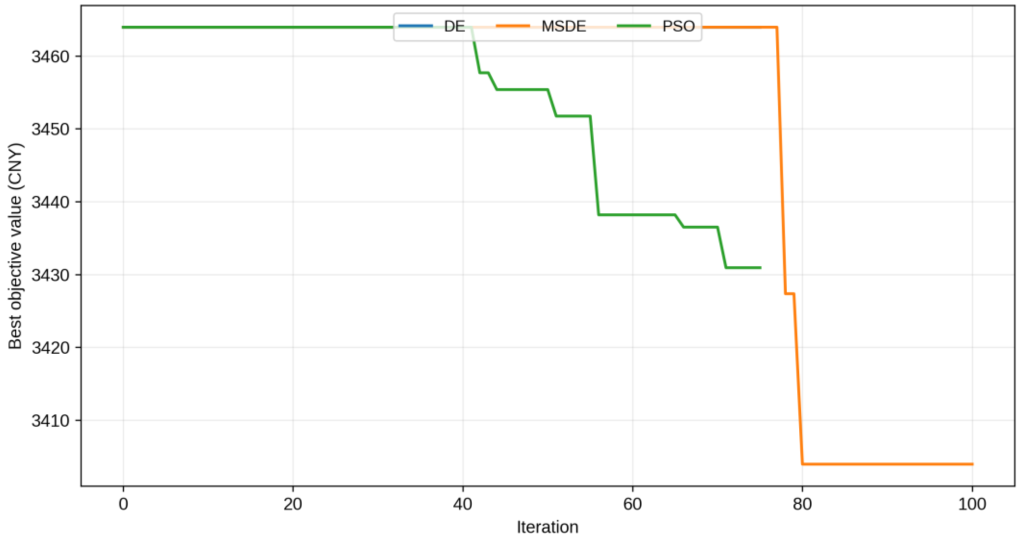

Figure 6: Convergence performance of different algorithms.

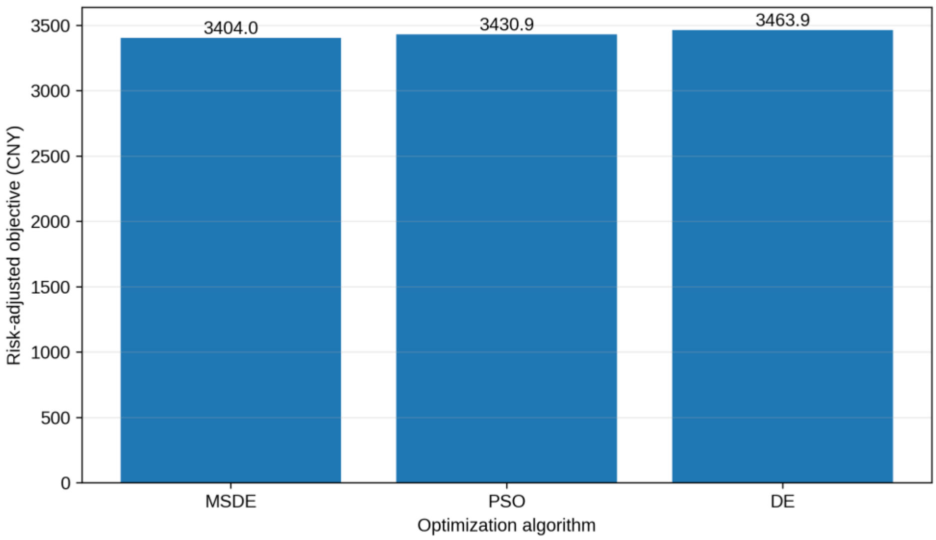

Figure 7: Scheduling results.

As shown in Table 1, the risk adjustment target value of the proposed algorithm is 3403.96 yuan, which is 59.98 yuan lower than the standard differential evolution algorithm and 26.97 yuan lower than the particle swarm optimization algorithm. Its expected operating cost and CVaR are also lower than the two comparative algorithms, indicating that the proposed algorithm can not only reduce the average operating cost but also reduce the economic risk in high-cost scenarios.

Table 1: Dispatch Results of Different Optimization Algorithms.

Algorithm	**Risk-Adjusted Objective Value (CNY)**	**Expected Cost (CNY)**	**CVaR (CNY)**	**Runtime (s)**	**Terminal SOC**
MSDE	3403.96	2796.50	3037.29	17.77	0.550
DE	3463.95	2844.08	3099.32	10.90	0.550
PSO	3430.93	2819.87	3055.32	10.55	0.551

Compared with the comparative methods, the running time of the proposed algorithm is slightly increased. This is because the algorithm further incorporates local Gaussian search, opposition learning, and multi-scenario fitness evaluation in the basic differential evolution process. However, for the 24-hour day-ahead scheduling problem, the computation time of 17.77 s is still within an acceptable range, and the increased computational overhead can be traded for lower operating costs and risk indicators.

4.6. Cost Composition Analysis

The cost composition of the optimal dispatch scheme is shown in Figure 8. The operating cost of the micro gas turbine is RMB 1295.35, and the grid interaction cost is RMB 1239.40, which constitute the main components of the total operating cost. Carbon emission costs are RMB 193.25, diesel generator operating costs are RMB 49.17, and energy storage degradation costs are RMB 19.11.

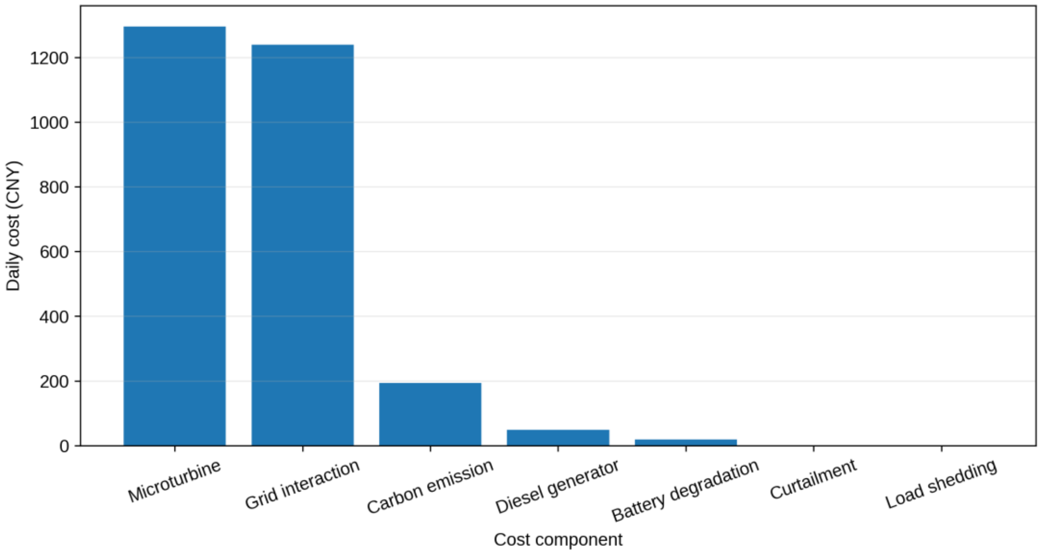

Figure 8: Operating cost composition.

The micro gas turbine and the grid handle most of the surplus load, hence their corresponding cost proportions are relatively high. Due to their higher unit power generation cost and carbon emission level, diesel generators are only put into operation during a few periods of power shortage, and their cost is significantly lower than that of the micro gas turbine and grid interaction costs. Under the baseline conditions, the costs of wind and solar curtailment and load shedding are both zero, indicating that the proposed dispatch strategy can fully utilize wind and solar energy and ensure power supply to the load while meeting equipment constraints.

4.7. Sensitivity Analysis of Wind and Solar Forecast Errors

To analyze the impact of renewable energy uncertainties on dispatch results, wind and solar forecast error levels were set to 5%, 10%, 15%, and 20%, respectively, and calculations were performed using the same energy storage plan under different error scenarios. The results are shown in Table 2.

Table 2: Scheduling results under different prediction error levels.

Forecast Error Level (%)	Expected Cost (CNY)	CVaR (CNY)	Risk-Adjusted Objective Value (CNY)	Cost Standard Deviation (CNY)	Average Load Shedding (kWh)
5	2758.46	2895.27	3337.52	75.09	0.00
10	2777.61	3228.09	3423.23	226.15	0.36
15	2891.73	3893.12	3670.35	411.18	1.43
20	3001.34	4688.53	3939.04	663.41	3.78

As the wind and solar forecasting error level increased from 5% to 20%, the expected operating cost increased from RMB 2758.46 to RMB 3001.34, and the CVaR increased from RMB 2895.27 to RMB 4688.53. Compared to the expected cost, the increase in CVaR was more significant, indicating that high-cost tail-end scenarios are more sensitive to renewable energy forecasting errors. When the error level is low, costs are relatively concentrated across scenarios; as the error increases, the standard deviation of costs increases from RMB 75.09 to RMB 663.41, significantly widening the economic differences between scenarios.

When the forecasting error reaches 10% or more, some low wind and solar output scenarios experience a small amount of load shedding, and the average load shedding increases with the error level. This indicates that under large forecasting deviations, the existing grid power purchase limit, controllable unit capacity, and energy storage regulation capacity may not be able to fully cover extreme power shortages. No wind or solar curtailment occurred at any of the error levels, indicating that the main risk currently facing the system comes from insufficient renewable energy output, rather than overcapacity.

5. Conclusion

This paper addresses the economic dispatch problem of grid-connected microgrids under uncertain wind and solar power output conditions. A 24-hour risk-based economic dispatch model is constructed, incorporating wind power, solar power, micro gas turbines, diesel generators, battery energy storage systems, and the public power grid. Multiple wind and solar power output scenarios are generated using a time-dependent prediction error model. The expected operating cost is combined with CVaR to establish a risk adjustment objective function that balances average economic efficiency and high-cost tail risk.

To improve the solution performance of the multi-scenario dispatch problem, this paper proposes the MSDE algorithm. Based on the standard DE algorithm, this algorithm introduces elite-guided mutation, adaptive parameter adjustment, local Gaussian search, and oppositional learning strategies, thus balancing early global exploration with later local development. Numerical results show that the risk adjustment objective value obtained by the multi-strategy adaptive differential evolution algorithm is 3403.96 yuan, lower than DE and PSO. Its expected operating cost and conditional risk value are also superior to the two comparative methods. Meanwhile, the energy storage SOC remains within acceptable limits, and the end-point SOC can recover to its initial level, indicating that the proposed method can achieve coordinated scheduling among wind and solar energy, energy storage, controllable generating units, and the public grid while meeting operational constraints.

Further sensitivity analysis shows that as the wind and solar prediction error level increases from 5% to 20%, the expected operating cost, conditional risk value, and scenario cost fluctuations all show an upward trend, with the conditional risk value increasing more significantly, indicating that high-cost scenarios at the tail end are more sensitive to new energy prediction errors. Therefore, it is necessary to introduce risk measurement in microgrid scheduling. This paper still has certain limitations, such as the lack of load and electricity price uncertainties in the model, the use of a linear approximation for energy storage lifetime decay, and the lack of discrete modeling for the start-up and shutdown states of controllable generating units. Future research could further consider multiple uncertainties, nonlinear energy storage degradation characteristics, and multi-timescale scheduling mechanisms to improve the applicability of the proposed method in complex microgrid operating scenarios.

References

[1] Shahzad S. Possibilities, challenges, and future opportunities of microgrids: A review[J]. Sustainability, 2023, 15(8): 6366.

[2] Talaat M. Artificial intelligence applications for microgrids integration and management of hybrid renewable energy sources[J]. Artificial Intelligence Review, 2023, 56(9): 10557-10611.

[3] Zheng K. Stochastic scenario generation methods for uncertainty in wind and photovoltaic power outputs: A comprehensive review[J]. Energies, 2025, 18(3): 503.

[4] Alguhi A A, Al-Shaalan A M. LSTM-based prediction of solar irradiance and wind speed for renewable energy systems[J]. Energies, 2025, 18(17): 4594.

[5] Osifeko M, Munda J. Scenario-Based Stochastic Optimization for Renewable Integration Under Forecast Uncertainty: A South African Power System Case Study[J]. Processes, 2025, 13(8): 2560.

[6] Mahalingam A. A survey of photovoltaic power forecasting approaches in solar energy landscape[M]//Computational Methods in Science and Technology. CRC Press, 2024: 87-101.

[7] Zheng K. Stochastic scenario generation methods for uncertainty in wind and photovoltaic power outputs: A comprehensive review[J]. Energies, 2025, 18(3): 503.

[8] Saidani K, Essaddi N, Besbes M. Long-Term Solar Energy Prediction With Robust Monte Carlo Simulation Method to Predict Solar Energy Using Univariate and Multivariate Time Series Models[J]. International Journal of Modeling, Simulation, and Scientific Computing, 2026.

[9] Sener N. Risk-Averse Green Hub Location Under Multi-Source Uncertainty: A CVaR-Based Model With Scenario Reduction[J]. IEEE Access, 2026, 14: 26621-26634.

[10] Deng G, Li K, Liang L. Robust optimization of pharmaceutical inventory under supply and demand uncertainty: a multi-period CVaR model based on the SPD framework[J]. Industrial Management & Data Systems, 2026: 1-27.

[11] Liu W. Elite elimination osprey optimization algorithm optimized kernel extreme learning machine for bankruptcy prediction problems[J]. Scientific Reports, 2026.

[12] Li C. Path planning problem solved by an improved black-winged kite optimization algorithm based on multi-strategy fusion[J]. International Journal of Machine Learning and Cybernetics, 2025, 16(10): 7859-7895.

[13] Xu H. A hybrid differential evolution particle swarm optimization algorithm based on dynamic strategies[J]. Scientific reports, 2025, 15(1): 4518.

[14] Singh A K, Kumar A. Hybrid multi-objective particle swarm optimization feature selection approach with firefly algorithm using decision tree classifier[J]. Evolutionary Intelligence, 2025, 18(2): 45.

[15] Hrinivich W T. Clinical VMAT machine parameter optimization for localized prostate cancer using deep reinforcement learning[J]. Medical physics, 2024, 51(6): 3972-3984.